Journal of Alloys and Compounds 509 (2011) 7854–7860

Contents lists available at ScienceDirect

Journal of Alloys and Compounds

journal homepage: www.elsevier.com/locate/jallcom

An investigation on linear optical properties of dilute Cr doped ZnO thin films synthesized via sol–gel process

A. Esmaielzadeh Kandjani[a,*], M. Farzalipour Tabriz[a], O. Mohammad Moradi[a], H.R. Rezaeian Mehr[a], S. Ahmadi Kandjani[b], M.R. Vaezi[a]

[a] Division of Nanotechnology and Advanced Materials, Materials and Energy Research Centre (MERC), Karaj, Iran
[b] Research Institute for Applied Physics and Astronomy, University of Tabriz, Tabriz, Iran

ARTICLE INFO

Article history:
Received 20 October 2010
Received in revised form 11 January 2011
Accepted 19 January 2011
Available online 28 January 2011

Keywords:
Semiconductors
Thin films
Sol–gel processes
Optical properties
Light absorption and Reflection

ABSTRACT

Cr doped ZnO thin films were prepared via sol–gel method. The effects of dopant concentration (0%, 1.5% and 3%) annealing temperature and film thickness on UV–Vis spectra of prepared films were investigated. Also, the thickness and surface topology of thin films were investigated by thickness profile meter (DEKTAK) and Atomic Force Microscopy (AFM), respectively. In addition, the band gap and Urbach energy of prepared films were calculated completely for the samples. The results showed that by increasing the dopant concentrations, the microstrain of the prepared thin film structures also increases while the band-gap values decrease. Meanwhile, an increase in annealing temperature makes a decrease in band gap and microstrain of thin films. The increase in thickness resulted in red shift in band gap and reduction in interior microstrains.

© 2011 Elsevier B.V. All rights reserved.

1. Introduction

Nowadays, wide band gap thin film semiconductors, among which ZnO has known to be promising candidate for different optoelectronic applications such as UV detectors, UV filters, solar cells, Light Emitting Diodes (LED), photocatalysts, etc. [1,2], are widely used in various applications ranging from biotechnological sensors to optoelectronics devices [3]. ZnO has a large exciton-binding energy of 60 meV and wide bandgap energy of 3.37 eV at room temperature in bulk form [4]. Existence of native defects such as zinc interstitials (Zn_i) and oxygen vacancies (V_O) in ZnO structure makes it an n-type semiconductor in undoped form [5,6]. Controlling these native defects becomes necessary when controlling the electrical and optical properties of produced ZnO thin films is required. There are technological difficulties in producing ZnO thin films with exact properties by chemical methods due to the complex relation between different synthetic variables in synthesizing procedure and the amount of native defects. Using metal doped zinc oxides has been attracting many researchers' attention due to its ability in controlling type and also carrier density of these semiconductors [7]. Trivalent elements such as Al [8], Ga [9], Cr [10] could be used as extrinsic elements for producing n-type ZnO with higher controllability on its electric conductivity and optical properties by varying their concentrations.

Among these dopants, Cr is an important transition metal element with closer ionic (Cr^{3+}) radius parameter to that of Zn^{2+}, which can penetrate into the ZnO crystal lattice or easily substitute the position of Zn^{2+} in the ZnO lattice [11]. Although optical properties of doped ZnO films have been delineated to a large extent, in-depth reports on studies of linear optical properties of Cr doped ZnO thin films are still few.

Controlling characteristics of coating (i.e. homogeneity, roughness and coat thickness) is important for tailoring final properties of semiconductors coatings [12]. Different approaches have been employed to produce ZnO thin films, including: Pulsed Laser Deposition (PLD) [13], Chemical Vapor Deposition (CVD) [14], Chemical Bath Deposition (CBD) [15] and sol–gel [16] methods. Sol–gel is known as an inexpensive chemical method with simple procedure, high thickness controllability and coating ability of large and complex shaped substrates. Various parameters, including temperature, medium pH, aging period, amount and type of modifier and hydrolysis agent, can change the morphology and lattice parameters of final products as well as their band structures [17].

In the present article, we report a simple method for synthesizing Cr doped ZnO thin films. The effects of dopant concentration, calcinations temperature and period and film thickness on optical properties of final zinc oxide coats were studied through atomic force microscopy (AFM) and thickness profile meter for surface analyses and UV–Vis spectroscopy for linear optical properties.

* Corresponding author. Tel.: +98 9144151594; fax: +98 411 5565295.
E-mail address: MSTGAhmad@Gmail.com (A.E. Kandjani).

0925-8388/$ – see front matter © 2011 Elsevier B.V. All rights reserved.
doi:10.1016/j.jallcom.2011.01.133

Table 1
Sol–gel variables for preparing ZnO thin films.

Sample	Annealing temperature (°C)	Number of coats	Dopant (atm%)
Z-1	200	1	0
Z-2	300	1	0
Z-3	400	1	0
Z-4	500	1	0
Z-5	200	1	1.5
Z-6	300	1	1.5
Z-7	400	1	1.5
Z-8	500	1	1.5
Z-9	200	1	3
Z-10	300	1	3
Z-11	400	1	3
Z-12	500	1	3
Z-13	400	2	0
Z-14	400	3	0
Z-15	400	2	3
Z-16	400	3	3

2. Experimental

2.1. Materials

Zinc acetate ($Zn(CH_3COO)_2{\cdot}2H_2O$), chromium nitrate ($Cr(NO)_3{\cdot}3H_2O$) and mono-ethanolamin (MEA) were purchased from Merck and used without any further purification.

2.2. Synthesis method

Zinc acetate with desired amounts of $Cr(NO)_3{\cdot}3H_2O$, as dopant, was firstly dissolved in methanol and mono-ethanolamin (MEA) solution at 50 °C. The concentration of zinc acetate was kept at 0.1 M and the weight ratio of MEA to zinc acetate was kept at 1.0. Then, the solution was aged for 24 h at 50 °C. A soda lime glass was used as substrate material washed with absolute acetone and methanol in an ultrasonic bath and then washed with deionized water. The glass substrates were dipped into the solution and withdrawn at the rate of 3.0 cm/min and the coated substrates were dried at 75 °C for 1 h in air. Then the coated glasses were annealed for 1 h in air. Annealing temperature, number of dip coating procedure and dopant concentration for producing ZnO thin films are listed in Table 1.

2.3. Analysis

The crystalline structures of materials were studied using a Unisuntis (XMD 300) X-ray diffractometer (XRD) with Cu-Kα radiation (λ = 0.154178 nm). The morphology of the film surface was analyzed by a Scientific (SB-4) atomic force microscope (AFM). To measure the thickness of thin layers, a thickness profile meter (DEKTAK 8000) was used. Linear optical properties of the samples were studied by double-beam Shimadzu UV-2450 Scan UV–Visible spectrophotometer.

2.4. Used equations

The surface topology of obtained zinc oxide thin films was analyzed using AFM. Also, to investigate the final roughness of the coats five roughness parameters were considered and analyzed including [18]: roughness average or arithmetic average of absolute values (R_a):

$$R_a = \frac{1}{n}\sum_{i=1}^{n}|h_i| \tag{1}$$

root mean square (R_q):

$$R_q = \sqrt{\frac{1}{n}\sum_{i=1}^{n}|h_i^2|} \tag{2}$$

peak-to-peak height or max height of profile (R_t):

$$R_t = R_p - R_v \tag{3}$$

surface skewness (R_{sk}):

$$R_{sk} = \frac{1}{nR_q^3}\sum_{i=1}^{n}|h_i^3| \tag{4}$$

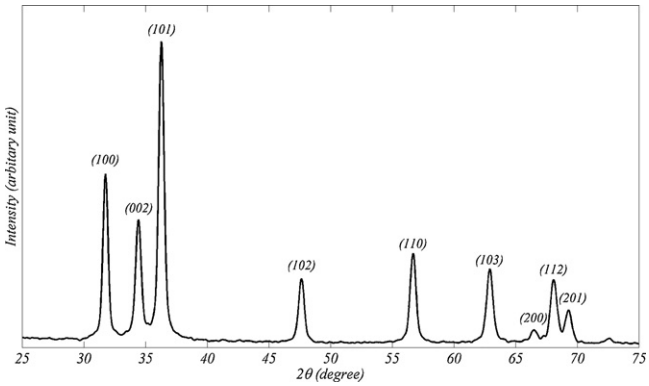

Fig. 1. XRD pattern of sample Z-3.

and surface kurtosis (R_{ku}):

$$R_{ku} = \frac{1}{nR_q^4}\sum_{i=1}^{n}|h_i^4| \tag{5}$$

where n is the number of obtained surface points and h_i is the height of ith element obtained from AFM analysis. Rp and Rv are maximum peak height and maximum valley depth, respectively. In particular, R_{sk} is a measure of the curve symmetry described as the height distribution, and can discriminate between wide valleys with narrow sharp peaks and high plateaus with sharp deep valleys. R_{ku} represents the height distribution through the 'peakedness' of the profile. A surface with a Gaussian height distribution has a kurtosis value of 3 and one with a narrow height distribution has a kurtosis value >3, while a kurtosis value of <3 relates to a surface that has a widely spread out height distribution.

Absorption coefficient ($\alpha(\lambda)$) can be derived from transmission spectra using [19]:

$$\alpha(\lambda) = \frac{1}{d}\ln\left(\frac{1}{T}\right) \tag{6}$$

where d is thickness of thin films obtained from DEKTAK thickness profile meter and T is transmission spectra of synthesized ZnO thin films. Also, absorption coefficient $\alpha(\lambda)$ of semiconductors is obtained by the following expression:

$$\alpha(\lambda) = A\frac{(h\nu - E_g)^{0.5}}{h\nu} \tag{7}$$

where A is coefficient of the given electronic transition probability. The $(\alpha h\nu)^2$ versus the photon energy $h\nu$ variation in the fundamental absorption region must be plotted to determine the E_g. Extrapolation of linear portion to the energy axis at $(\alpha h\nu)^2 = 0$ gives the E_g value.

The absorption coefficient α near band edge varies exponentially with photon energy. It would be assumed that the spectral dependence of the absorption edge is in accordance with Urbach formula [20]:

$$\alpha(\lambda) = \alpha_0 \cdot \exp\left[\frac{h\nu}{E_0}\right] \tag{8}$$

where α_0 is the Urbach absorption at the edge and E_0 is the Urbach energy width weakly dependant on temperature and believed to be a function of the structural disorder. E_0 values were estimated from the slopes of the linear plot of $\ln(\alpha)$ against $h\nu$.

3. Results and discussion

3.1. XRD and AFM analysis

The XRD pattern of Z-3 as a typical sample is shown in Fig. 1. All peaks are attributed to wurtzite ZnO (JCPDF 36-1451) and no peak of other crystalline phases was detected. As shown in this figure, (1 0 1) plane sets have the highest intensity and the intensity order of peaks were similar in all other samples.

Fig. 2 shows the AFM images of samples Z-3, Z-7 and Z-11. By using Eqs. (1)–(5), the roughness parameters, analyzed through AFM, are listed in Table 2. By an increase in dopant concentration the average roughness of the film increases slightly while the thicknesses are close to each other and equal to 74 ± 2 nm.

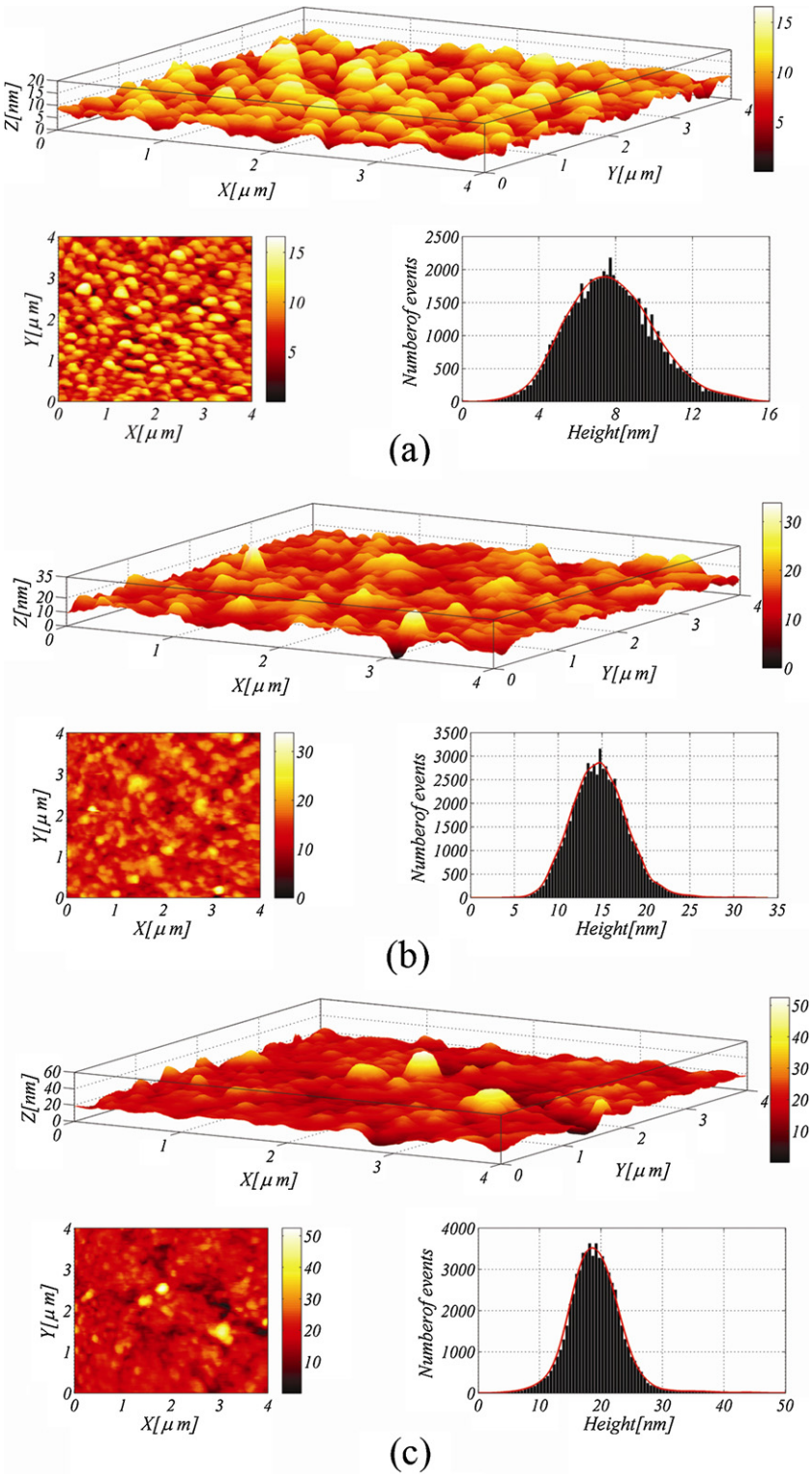

Fig. 2. The AFM images of ZnO films, (a) Z-3, (b) Z-7 and (c) Z-11. The 3D and 2D AFM images are shown with the histograms of height distribution of the coatings.

Table 2
The thickness and roughness parameters from the surface analysis of AFM topography.

Sample	R_a [nm]	R_q [nm]	R_t [nm]	R_{sk} [nm]	R_{ku} [nm]	Thickness [nm]
Z-3	7.76	8.0841	16.59	1.1174	1.3277	74
Z-7	14.7055	15.0493	33.87	1.0695	1.1948	73
Z-11	19.1375	19.6902	52.52	1.0928	1.2826	75
Z-13	24.395	25.2813	46.13	1.1015	1.2801	95
Z-14	32.0441	33.0078	69.85	1.0872	1.2441	147

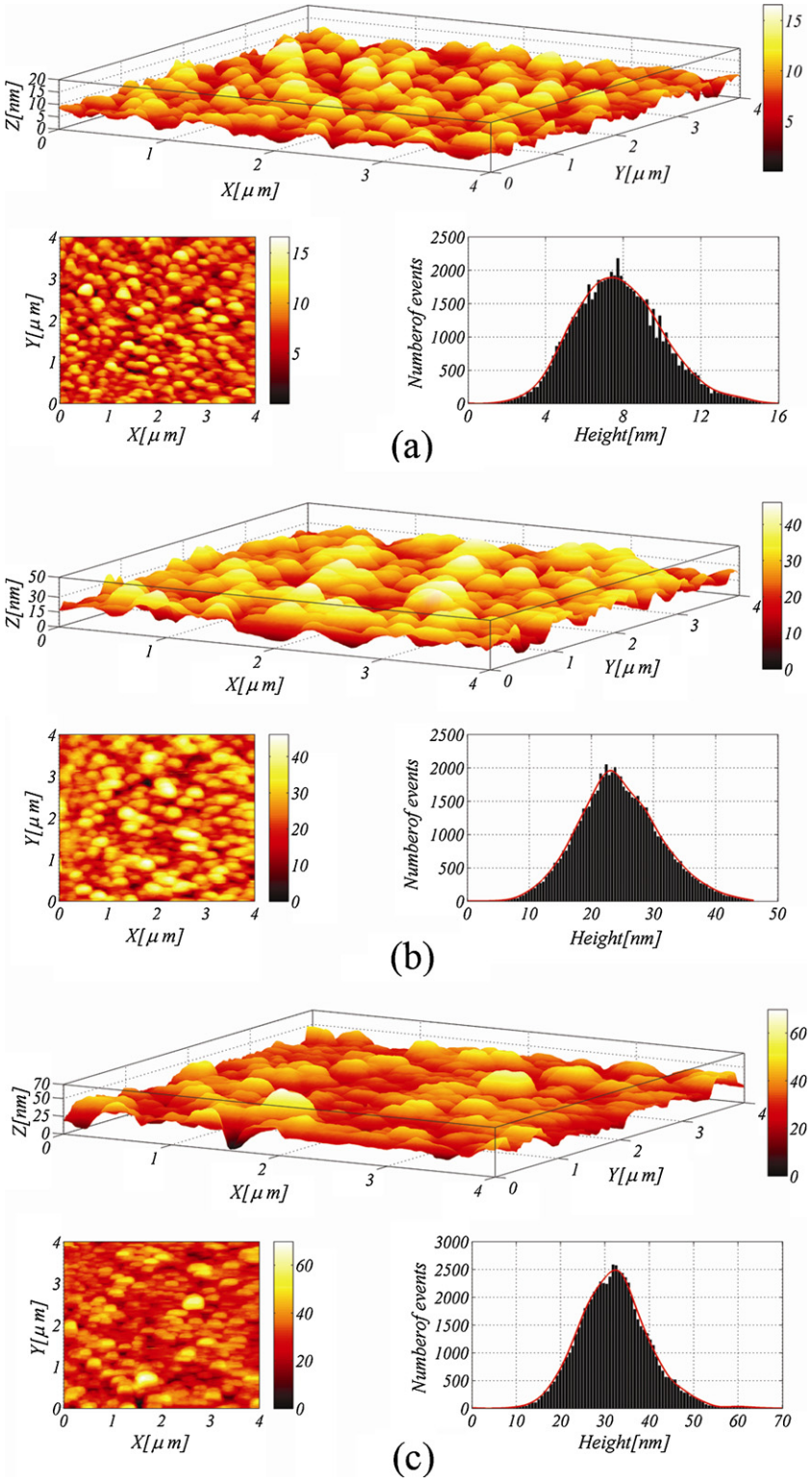

Fig. 3. The AFM images of ZnO films, (a) Z-3, (b) Z-13 and (c) Z-14. The 3D and 2D AFM images are shown with the histograms of height distribution of the coatings.

Fig. 3 shows the AFM images of Z-3, Z-13 and Z-14. According to these images and Table 2, with an increase in the number of applied dipping steps, the thickness and the roughness of the thin films were increased. This could be resulted from the growth of surface crystallites during the calcinations process and subsequence increase in layer thicknesses of sol–gel derived ZnO thin films [21].

3.2. The effect of annealing temperature on linear optical properties of ZnO:Cr films

The transmission spectra in the range of 350–800 nm at room temperature for doped and undoped ZnO thin films at different annealing temperatures are shown in Fig. 4. All films exhibit high transmission in the studied UV–Vis range. Through Eq. (7),

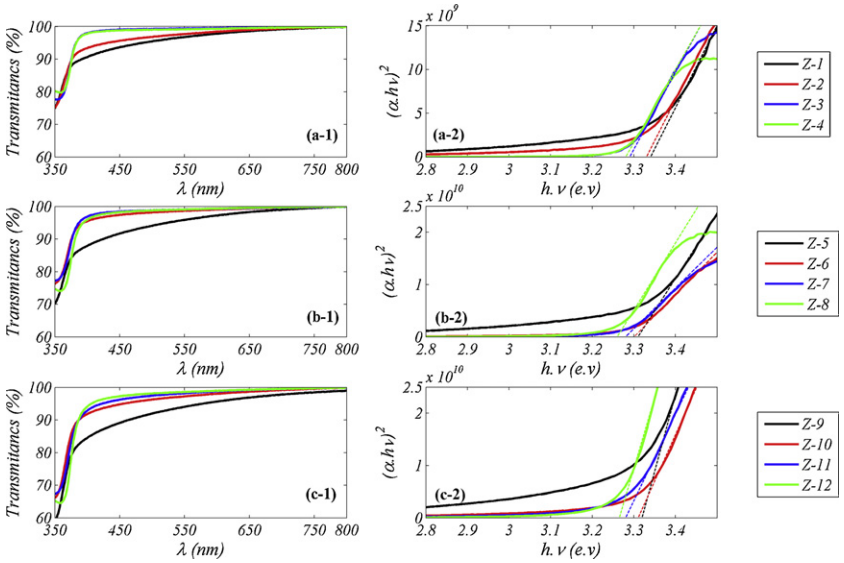

Fig. 4. The transmission spectra and variations of $(\alpha h\nu)^2$ versus the photon energy $h\nu$ for ZnO thin films with (a) 0, (b) 1.5 and (c) 3% Cr.

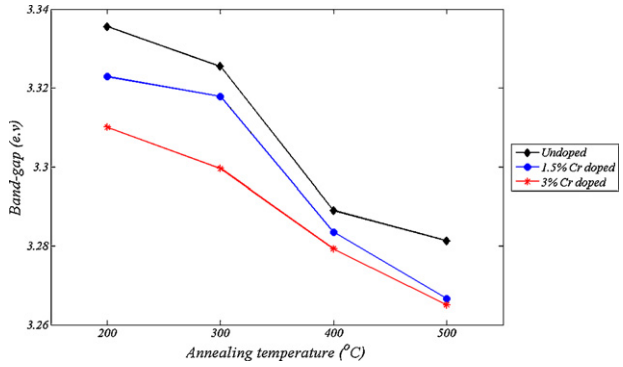

Fig. 5. Band gap variation by varying annealing temperature.

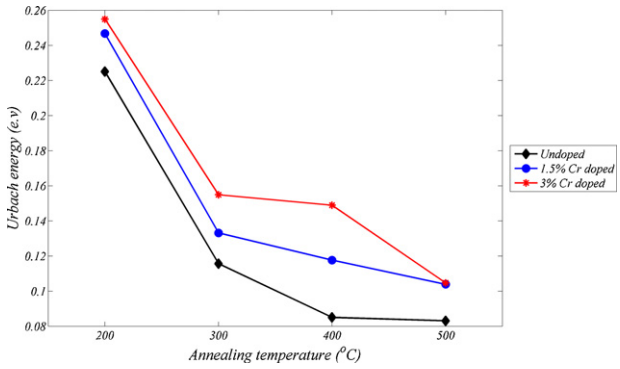

Fig. 7. Urbach energy of the ZnO films with different dopant concentrations as a function of the annealing temperature.

absorption coefficients ($\alpha(\lambda)$) of thin films were obtained from their transmission spectra. Using Eq. (8), the bandgap of obtained ZnO thin films was driven from their spectra. By an increase in the dopant concentration due to increase in surface roughness (Table 2), the absorption edge becomes less sharp [22].

The obtained E_g versus annealing temperature for coatings with different dopant concentrations are shown in Fig. 5. As seen in this figure by increasing the annealing temperature, the band gap decreases. This red shift could be related to subsequence growth of ZnO crystallites due to increase in annealing temperature. Also, by an increase in dopant concentration band gap values of thin films show a decrease. This observation have a good agreement with Chang-feng et al. work where they reported red shift for Cr doped

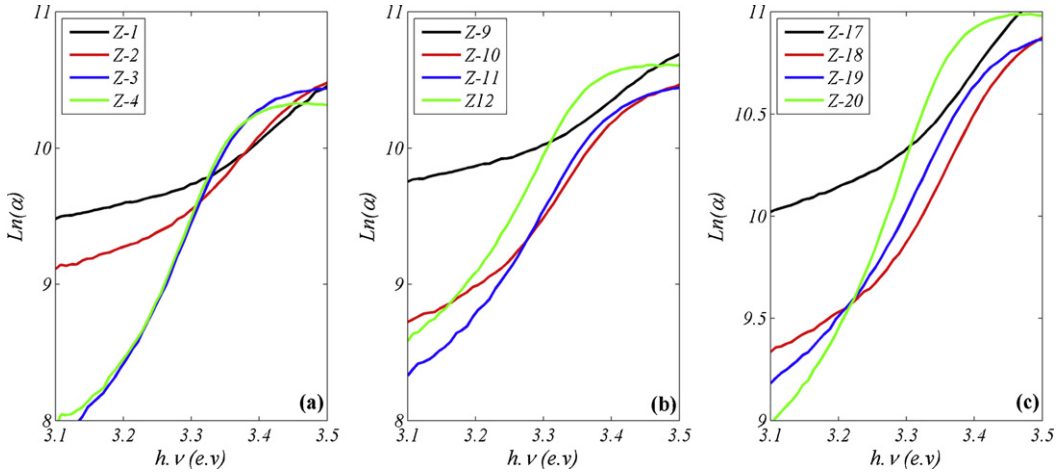

Fig. 6. The Urbach plots of the ZnO thin films with (a) 0, (b)1.5 and (c) 3% Cr.

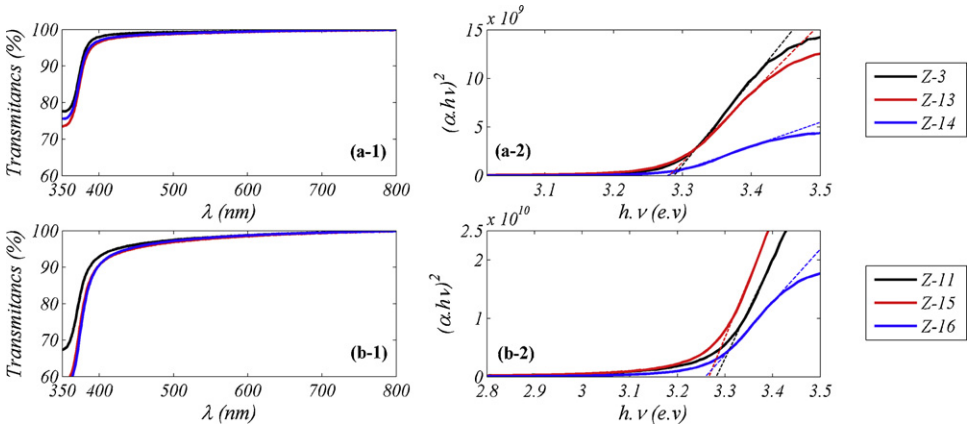

Fig. 8. The transmission spectra and variations of $(\alpha h\nu)^2$ versus the photon energy $h\nu$ for ZnO thin films with (a) 0 and (b) 3% Cr.

ZnO thin films [23]. This phenomenon could be resulted from the fact that the excess Cr doping degenerates the crystal quality of ZnO films.

To obtain the Urbach energy of obtained films, as shown in Fig. 6, the variation of $\ln(\alpha)$ against $h\upsilon$ near band edge of obtained thin films was plotted.

The calculated Urbach energies from Eq. (8) are shown in Fig. 7. Any increase in the annealing temperature, results in decrease of the Urbach energy. As mentioned above, the increase in annealing temperature results in growth and also reduction of defects of the obtained films. But, by an increase in Cr dopant the distortion in ZnO crystallites increases due to exerting the dopant atoms into wurtzite structure of zinc oxide. Doped Cr^{3+} atoms occupy the position of Zn^{2+} in ZnO crystals and changes the lattice constants and consequently increase the lattice distortions [24].

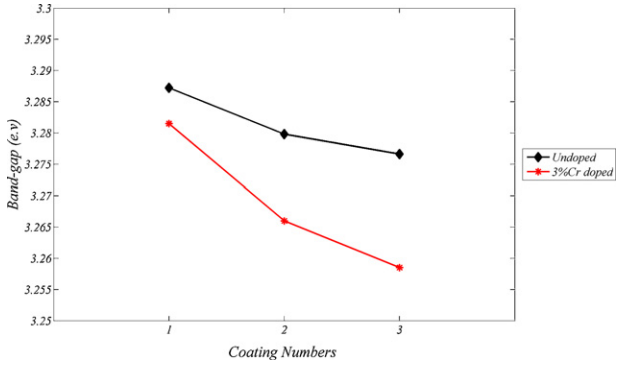

Fig. 9. Band gap variation by varying coating layer numbers.

3.3. The effects of applied dip coating layers numbers on linear optical properties of ZnO:Cr films

The transmission spectra for prepared ZnO thin films with different thicknesses are shown in Fig. 8. As could be seen from these figures, all the films exhibit high transmission in the studied UV–Vis range but by any increase in thickness of thin films the optical transmission decreases. Also the band gaps of prepared thin films are obtained using Eqs. (7) and (8) as shown in part 2 of Fig. 8.

The obtained band gap variation by coating layer numbers for undoped and 3% Cr doped samples is shown in Fig. 9. As illustrated in this figure, the band gap decreases with increasing film thickness. The band gap of doped films is less than undoped ones. The reason for this phenomenon was already discussed.

To obtain Urbach tail of the films, the variation of $\ln(\alpha)$ against $h\upsilon$ near band edge of obtained thin films was plotted, as shown in Fig. 10.

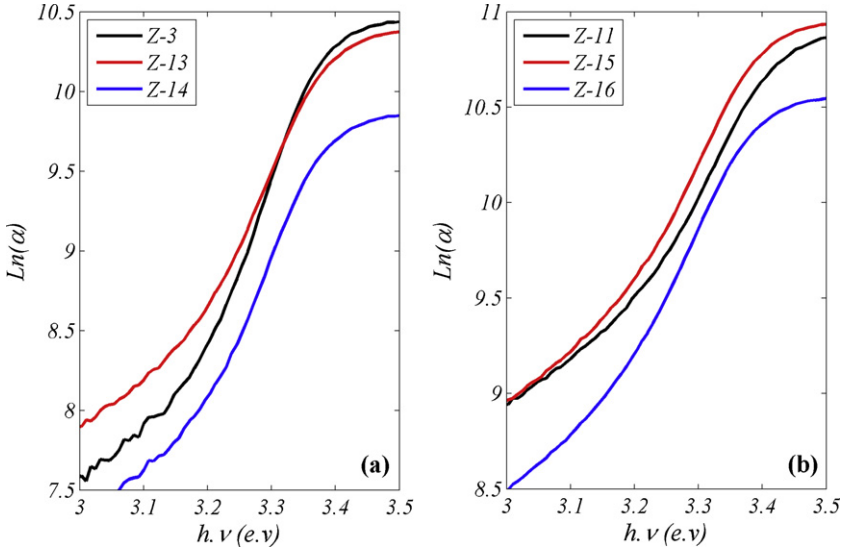

Fig. 10. The Urbach plots of the ZnO thin films with (a) 0 and (b) 3% Cr.

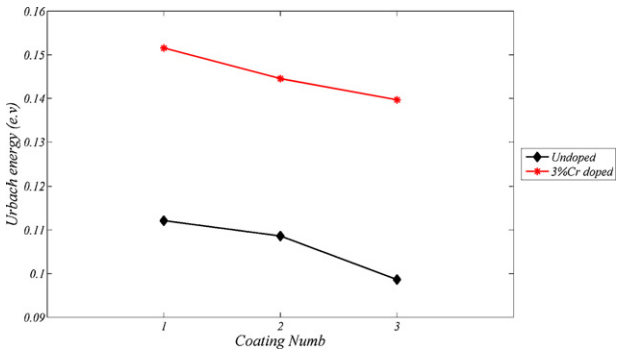

Fig. 11. Urbach energy of the ZnO films with different dopant concentrations as a function of applied dip coating layers numbers.

The variation of Urbach energies with changing thicknesses of the films is shown in Fig. 11. As could be seen from this figure, by increasing the thickness of ZnO film, the Urbach energy decreases. The high amounts of Urbach energies show the poor crystallinity of the samples which means there is a large number of defects in the film structures. Oztas et al. showed that an increase in film thickness results in an increase in the crystallite size of ZnO thin films by a columnar growth of crystallites. The growth of crystallite size is due to predominant recrystallization process and reduction of lattice imperfection [25]. Thus, by an increase in the film thickness the film tends to be crystallized with less disordering sites. This phenomena affects the band gap and also, a decrease in the band gap could be resulted from the same phenomenon, i.e. by an increase in film thickness, ordering of the film structure (crystallinity of the film) and crystallite sizes of the film both increases and consequently the band gap decreases. Also, as shown in Fig. 8, in the thicker films, absorption edge becomes less sharp, which could be resulted two phenomena: first, by increasing the film thickness, via applying additional dipping steps in coating procedure, bigger crystallites are formed; and, second, an increase in the film thickness results increase of surface roughness of the coatings (as listed in Table 2) which consequently increases scattering areas of the surface.

4. Conclusion

The ZnO thin films were synthesized via a simple sol–gel process with different dilute Cr dopant concentrations. The effects of three synthetic parameters including: doping concentration, annealing temperature and film thickness on optical absorption and surface topology of thin films were investigated thoroughly. The results could be summarized as following:

- By increasing in dopant concentration the average roughness of the film increases slightly while the thickness remains constant.
- By an increase in the number of applied dip coating, film thickness increases from 74 nm (after 1 procedure dip coating) to 147 nm (3 procedures dip coating), which results in an increase in the roughness of the films.
- By an increase in dopant concentration and film thickness, the absorption edge becomes less sharp.
- An increase in dopant concentration results in a decrease in band gap values while the interior microstrain shows an increase.
- An increase in annealing temperature results in decrease in band gap values and interior microstrains of thin films.
- By an increase in the number of applied dip coating, film thickness increases from 74 nm (after 1 procedure dip coating) to 147 nm (3 procedures dip coating) and band gap values and interior microstrains of thin films show a decrease.

References

[1] R. Konenkamp, R.C. Word, M. Godinez, Nano Letters 5 (2005) 2005–2008.
[2] M. Law, L.E. Greene, J.C. Johnson, R. Saykally, P.D. Yang, Nat. Mater. 4 (2005) 455–459.
[3] K. Takahashi, A. Yoshikawa, A. Sandhu, Wide Bandgap Semiconductors, Fundamental Properties and Modern Photonic and Electronic Devices, Springer, Berlin, Heidelberg, USA, 2006.
[4] Ü. Özgür, Ya.I. Alivov, C. Liu, A. Teke, M.A. Reshchikov, S. Doğan, V. Avrutin, S.J. Cho, H. Morkoç, J. Appl. Phys. 98 (2005) p041301.
[5] S.B. Zhang, S.H. Wei, A. Zunger, Phys. Rev. B 63 (2001) 075205.
[6] C.G. Van de Walle, Phys. Rev. Lett. 85 (2000) 1012–1015.
[7] S.M. Sze, K.K. Ng, Physics of Semiconductor Devices, 3rd ed., John Wiley & Sons, Inc., USA, 2007.
[8] B.E. Sernelius, K.F. Berggren, Z.C. Jin, I. Hamberg, C.G. Granqvist, Phys. Rev. B 37 (1988) 10244.
[9] L.J. Mandalapu, F.X. Xiu, Z. Yang, J.L. Liu, Solid State Electron. 51 (2007) 1014–1017.
[10] S. Singh, E.S. Kumar, M.S. Ramachandra Rao, Scripta Mater. 58 (2008) 866–869.
[11] B.K. Roberts, A.B. Pakhomov, V.S. Shutthanandan, J. Appl. Phys. 97 (2005) 10–310.
[12] T. Wolkenstein, Electronic Processes on Semiconductor Surfaces During Chemisorptions, Plenum Press, USA, 1991.
[13] X.Q. Wei, Z. Zhang, Y.X. Yu, B.Y. Man, Opt. Laser Technol. 41 (2009) 530–534.
[14] Y. Kashiwaba, F. Katahira, K. Haga, T. Sekiguchi, H. Watanabe, J. Cryst. Growth 221 (2000) 431–434.
[15] C.D. Lokhande, P.M. Gondkar, R.S. Mane, V.R. Shinde, S.H. Han, J. Alloy Compd. 475 (2009) 304–311.
[16] D. Mondelaers, G. Vanhoyland, J. Sol–Gel Sci. Technol. 26 (2003) 523–526.
[17] C.J. Binker, G.W. Scherer, Sol–Gel Science: The Physics and Chemistry of Sol–Gel Processing, Academic Press Inc., UK, 1990.
[18] M. Pelliccione, T.M. Lu, Evolution of Thin Film Morphology: Modeling and Simulations, Springer, Berlin, Heidelberg, USA, 2008.
[19] C. Klingshirn, Semiconductor Optics, 2nd ed., Springer, Berlin, Heidelberg, USA, 2005.
[20] F. Urbach, Phys. Rev. 92 (1953) 1324.
[21] S. Lalitha, R. Sathyamoorthy, S. Senthilarasu, A. Subbarayan, K. Natarajan, Sol. Cells 82 (2004) 187–199.
[22] S.A. Mahmoud, A.A. Akl, KamalF H., Abdel-HadyF K., K. Natarajan, Physica B 311 (2002) 366–375.
[23] F.U. Chang-feng, C.H.E.N. Xi-ming, L.I. Lan, H.A.N. Lian-fu, W.U. Xiaoguo, Optoelectron. Lett. 6 (2010) 37–40.
[24] Y.M. Hu, Y.T. Chen, Z.X. Zhong, C.C. Yu, G.J. Chen, P.Z. Huang, W.Y. Chou, J. Chang, C.R. Wang, Appl. Surf. Sci. 254 (2008) 3873.
[25] M. Öztas, M. Bedir, Thin Solid Films 516 (2008) 1703–1709.